Computer Methods in Biomechanics and Biomedical Engineering, 2013
Vol. 00, No. 0, 1–14, http://dx.doi.org/10.1080/10255842.2012.761693

Taylor & Francis
Taylor & Francis Group

Sensitivity analysis of a cemented hip stem to implant position and cement mantle thickness

J. Shi[a], M. Browne[a]*, M. Strickland[a], G. Flivik[b] and M. Taylor[a,c]

[a]*Engineering Sciences Unit, Faculty of Engineering and the Environment, University of Southampton, Southampton SO17 1BJ, UK;* [b]*Department of Orthopedics, Skane University Hospital, Lund University, S-221 85 Lund, Sweden;* [c]*School of Computer Science, Engineering and Mathematics, Medical Device Research Institute, Flinders University, Sturt Road, Bedford Park, Adelaide SA 5042, Australia*

(*Received 30 March 2012; final version received 19 December 2012*)

Patient-specific finite element models of the implanted proximal femur can be built from pre-operative computed tomography scans and post-operative X-rays. However, estimating three-dimensional positioning from two-dimensional radiographs introduces uncertainty in the implant position. Further, accurately measuring the thin cement mantle and the degree of cement–bone interdigitation from imaging data is challenging. To quantify the effect of these uncertainties in stem position and cement thickness, a sensitivity study was performed. A design-of-experiment study was implemented, simulating both gait and stair ascent. Cement mantle stresses and bone–implant interface strains were monitored. The results show that small variations in alignment affect the implant biomechanics, especially around the most proximal and most distal ends of the stem. The results suggest that implant position is more influential than cement thickness. Rotation around the medial–lateral axis is the dominant factor in the proximal zones and stem translations are the dominant factors around the distal tip.

Keywords: total hip replacement; sensitivity; finite element analysis; design-of-experiment; implant alignment

1. Introduction

The predominant failure mode for cemented total hip replacement (THR) is aseptic loosening of the femoral stem (Herberts and Malchau 1997, 2000; Van Goethem and Pfluger 2005). Many studies have been performed to determine the stress distribution in the cement and at the implant–cement interface (Verdonschot and Huiskes 1997; Stolk et al. 2001, 2003; Pérez et al. 2006; Waanders et al. 2011). The performance of cemented THR is dependent on a number of factors including patient-specific bone geometry (Jonkers et al. 2008), bone material properties (Schileo et al. 2007), loading (Huiskes 1990; Pancanti et al. 2003), stem design (Nicolella et al. 2006; Dopico-Gonzalez et al. 2010; Ishida et al. 2011), stem positioning (Kleemann et al. 2003; Bah et al. 2011) and cement mantle thickness (Hernigou et al. 2009).

Direct verification of finite element (FE) predictions using clinical outcomes has rarely been performed. Lennon et al. (2007) computed accumulated damage, inducible displacement and migration of seventeen THR patient-specific FE models, five of the six early revisions had the highest migration prediction. The et al. (2008) quantified the association between the estimated hip joint contact force in biomechanical models and clinically measured wear rates using roentgen stereophotogrammetric analysis (RSA). The predicted maximum joint contact force and wear were clearly correlated in the first year post-operatively. Perillo-Marcone et al. (2004) predicted the implant migration using patient-specific FE models compared with clinical RSA data. Lengsfeld et al. (2005) investigated femoral strain changes after total hip arthroplasty from FE analysis based on a retrospective computerised tomography (CT) *in vivo* data set of 11 patients 12 years after THR. There was a significant reduction of the strain energy density values in all Gruen zones with the greatest effect near the distal tip of the stem. Turner et al. (2005) combined bone remodelling theory with FE models to predict alteration in periprosthetic apparent density; theoretical bone density changes correlated significantly with clinical densitometry measurements 2 years post-operatively.

For any such verification of patient-specific FE models of THR from clinical data, accurate stem positioning is essential. In many studies, post-operative radiographs are used for stem positioning. Therefore, it is only possible to position the stem accurately in the imaging plane, typically in the coronal plane. The objective of the present sensitivity analysis is to investigate the influence of the resulting uncertainty in out-of-plane THR stem position on the FE predictions of cement mantle stresses and bone–implant interface strains.

When generating patient-specific FE models, assumptions are made regarding the thickness and morphology of the cement mantle. Conventional cementing techniques result in a layer of pure cement and layer of cement interdigitated with bone. This bone–cement composite layer enhances the bonding strength of the cemented

*Corresponding author. Email: doctor@soton.ac.uk

implant (Stone et al. 1996; Lucksanasombool et al. 2003; Waanders et al. 2010). The thickness of this composite layer can vary, and it is often excluded from FE models of THR, as most studies simply model a pure cement mantle of uniform thickness (Ramaniraka et al. 2000; Janssen et al. 2005; Kumar et al. 2009; Pérez et al. 2009). For example, Kovanda et al. (2009) modelled cemented THR with four different stem designs: a pure cement mantle was modelled which was 4–7 mm thick in the proximal region and 1–3 mm thick in the distal region. Conventional surgical procedure aims to obtain a total cement mantle of 3–5 mm around the implant (Hernigou et al. 2009), since thin and deficient mantles have been associated with adverse clinical outcomes (Star et al. 1994; Massoud et al. 1997). This sensitivity study therefore also investigates the influence of estimated bone–cement composite layer thickness on the predicted cement mantle and cement–bone interface strains.

2. Method

2.1 Model construction

A FE model of an implanted proximal femur was generated (Figure 1) for one subject (female, 79 years, 76 kg) who had received a cemented femoral stem. The proximal femur geometry was segmented from pre-operative CT scans (resolution $0.43 \times 0.43 \times 1$ mm). The resulting bone model was implanted with a cemented MS30® femoral stem (Zimmer®, Warsaw, IN, USA). The cement mantle was modelled as a unified body with two regions: a layer of pure cement (at least 1 mm thick) and a bone–cement composite layer of varying thickness. The 'neutral' implant position was based on the post-operative coronal radiograph. The bone geometry segmentation and Boolean operations between stem, cement and bone were performed in Avizo® 6 (Visualization Sciences Group, Bordeaux, France). Customised scripts were used to position the implant and to perform Boolean operations to generate the implant cavity, cement layer and bone–cement composite layer. In the coronal plane, the stem was accurately aligned with the post-operative X-ray image. In the other planes, the neutral position was estimated using the neck axis and femur long axis as a guide.

The moduli were defined as 210 GPa for the implant and 2.8 GPa for bone cement (Coultrup 2010). Apparent bone density (ρ, g/cm^3) was calculated from CT voxel intensity [Hounsfield units (HU)] using calibration phantoms within the CT scans. The two calibration points that describe this linear relationship were (150 HU, 0.134 g/cm^3) and (350 HU, 0.329 g/cm^3). Young's modulus was then derived from bone apparent density (Morgan et al. 2003). Although Equation (1) was developed from the test results of femoral neck trabecular bone, it has been shown that numerical predictions using this constitutive law provided good agreement with experimental measurements (Schileo et al. 2007). A Poisson's ratio of 0.3 was applied for all materials.

$$E_b = 6.95\rho_{app}^{1.49}. \quad (1)$$

The minimum and maximum apparent bone densities were 0 and 1.63 g/cm^3 respectively. Within the bone tissue, the maximum Young's modulus was 14.35 GPa and Young's moduli which were calculated to be <10 MPa were thresholded to 10 MPa.

The Young's modulus of the bone–cement composite was derived using Voigt's composite model relationship:

$$E = E_b V_b + E_c(1 - V_b), \quad (2)$$

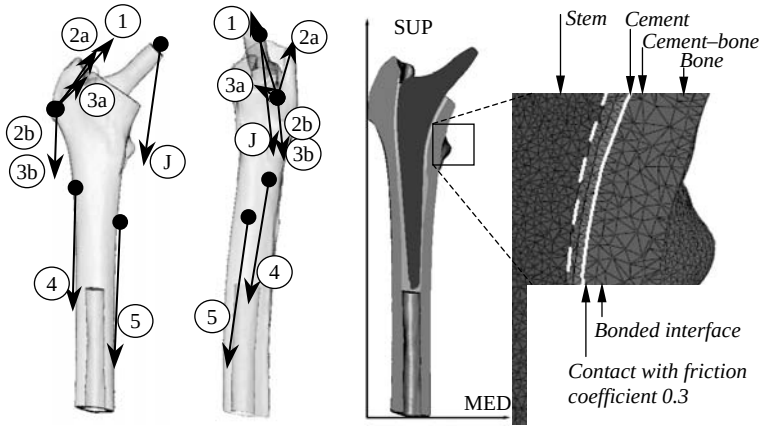

Figure 1. Orientation of FE model and (inset) structure of THR implantation. Three axes are along anterior/posterior (AP), medial/lateral (ML) and superior/inferior (SI). The positive directions of the three axes are medial (MED), anterior (ANT) and superior (SUP).

$$V_b = \frac{\rho_{app}}{\rho_t}, \quad (3)$$

where E_b and E_c represent the Young's modulus of bone and cement respectively, V_b is the volume-fraction of bone, ρ_{app} is bone apparent density and ρ_t is solid bone tissue density (2.18 g/cm^3 after Hernandez et al. 2001; Schileo et al. 2007). This composite model only applies to cancellous bone; unmodified CT-based properties were applied where the cement would otherwise 'interdigitate' into cortical bone. Note, cortical and cancellous regions were differentiated based on CT segmentation.

The model was meshed and assigned linear elastic material properties in Avizo (average element size ~1 mm, with ~538,000 tetrahedral elements) and then imported into ABAQUS® (SIMULIA, USA). 'Peak' loads associated with two representative daily activities (gait and stair ascent) were applied to the FE model, using joint and muscle forces from published musculoskeletal studies (Heller et al. 2005). Loads were expressed as a fraction of body weight and with respect to a standardised reference coordinate system (Bergmann et al. 1993). The load values are listed in Table 1 and load directions are displayed in Figure 1. The distal surface of the proximal femur was rigidly fixed. The interfaces between the bone and cement mantle (including the bone–cement composite region) were fully bonded, and the interface between stem and cement was modelled as de-bonded with a contact friction coefficient of 0.3 (Viceconti et al. 2000).

A mesh sensitivity study was performed by varying the element sizes of the cement and bone (Table 2). The variations of cement stresses were within 5% for different cement element sizes and the variations of equivalent bone strain at the bone–cement interface were within 5% for different bone element sizes.

2.2 *Sensitivity analysis*

A sensitivity study was performed using a design-of-experiment (DOE) approach to adjust the input factors (stem position and bone cement composite thickness). The stem was allowed to rotate about the superior–inferior (ROT_{SI}) axis and medial–lateral (ROT_{ML}) axis (these rotations were applied relative to the bottom tip of the stem due to the presence of a centraliser), as well as translate medial–laterally (TRN_{ML}) and anterior–posteriorly (TRN_{AP}). Bone–cement composite thickness was varied from 1–3 mm (Isaac et al. 2000). C_{THICK} represents the whole cement mantle thickness, including the 1 mm pure cement layer; total cement thickness therefore varies from 2–4 mm. Medial–lateral translation is not out-of-plane for a two-dimensional (2D) radiograph, but because this factor brings the stem into close proximity with the cortical bone, it was included as an additional factor, although with a smaller range of variation (2.5 mm total vs 5 mm total for TRN_{AP}). Table 3 summarises the variability assigned to these sensitivity factors. The ranges of these stem positions were tested to satisfy that the stem would not penetrate through the bone cortex. Twenty-five DOE trials were modelled. Three output measures were chosen for this sensitivity study. Table 4 summarises the FE output measures.

Table 1. Hip joint forces and muscle forces applied in the sensitivity study models.

Force	Gait (%BW)	Stair climbing (%BW)
Hip contact	237.75	251.05
Abductor (1)	104.23	113.80
Ilio-tibial tract, proximal part (2a)	0	16.83
Ilio-tibial tract, distal part (2b)	0	16.83
Tensor fascia latae, proximal part (3a)	18.99	6.48
Tensor fascia latae, distal part (3b)	19.02	6.51
Vastus lateralis (4)	94.73	136.96
Vastus medialis (5)	0	270.16

Von Mises stress of the cement mantle was chosen as a measure of potential fatigue failure of the cement mantle (Nicolella et al. 2001). Failure at the cement–stem and cement–bone interfaces may result from the occurrence of abnormally high shear and compressive stresses within the cement, leading to fracture of the cement and subsequent subsidence of the stem (Ramaniraka et al. 2000).

First principal stress of the cement mantle was used as a measure of tensile failure of cement (Harrington et al. 2002; Nicolella et al. 2006). Depending upon composition and curing, the ultimate tensile strength and compressive strength of cement have been reported to range from 24 to 49 MPa and 73 to 117 MPa, respectively (Lewis 1997).

The mechanical response of the bone itself was estimated by measuring equivalent strain at the bone–cement interface. Bone failure has been shown to be driven by deformation (Nalla et al. 2003; Taylor 2003), with high strain at the bone–cement interface being associated with implant migration (Taylor et al. 1998). The yield strain of cancellous bone has been reported to occur at 7000 microstrain (Morgan and Keaveny 2001).

'Peak' values were represented using the 95th percentile instead of the maximum value in the FE model, since individual maxima in elements are prone to numerical artifacts and singularities (Lennon and Prendergast 2001). For the von Mises stress and first principal stress of the cement mantle, 95% of the cement *volume* has stress less than the 95th percentile value. For equivalent strain at the bone–cement interface, 95% of the bone–cement interface *area* has strain less than the 95th percentile strain value. The 75th percentile and median stress/strain were also calculated; however, for all factors, similar trends were found for median, 75th percentile and

Table 2. Different meshes of implanted hip model and results with stair ascent peak load.

Cement element size	Bone element size	Total elements	Total nodes	95th Von Mises stress in cement (MPa)	95th Equivalent strain at bone–cement interface (10^3 μ strain)
1.5	3	357,193	77,514	4.8	1.92
1.5	2	391,166	83,098	4.83	2.04
1	3	394,255	83,779	5.07	1.93
1	2	526,277	105,883	4.97	2.06
0.7	2	1,010,413	188,815	4.98	2.04

Table 3. List of test conditions for 25 DOE trials.

Test no.	ROT_{SI} (°)	ROT_{ML} (°)	TRN_{AP} (mm)	TRN_{ML} (mm)	C_{THICK} (mm)
1	−5	0	0	−1.5	2
2	−5	0	0	−1.5	3
3	−5	0	0	−1.5	4
4	−5	3	2.5	0	2
5	−5	3	2.5	0	3
6	−5	3	2.5	0	4
7	0	−3	0	0	2
8	0	−3	0	0	3
9	0	−3	0	0	4
10	0	0	2.5	−2.5	2
11	0	0	2.5	−2.5	3
12	0	0	2.5	−2.5	4
13	0	3	−2.5	−1.5	2
14	0	3	−2.5	−1.5	3
15	0	3	−2.5	−1.5	4
16	5	−3	2.5	−1.5	2
17	5	−3	2.5	−1.5	3
18	5	−3	2.5	−1.5	4
19	5	0	−2.5	0	2
20	5	0	−2.5	0	3
21	5	0	−2.5	0	4
22	5	3	0	−2.5	2
23	5	3	0	−2.5	3
24	5	3	0	−2.5	4
25	0	0	0	0	2

95th percentile values. Therefore only 95th percentiles will be discussed in the following results.

To investigate the influence of input factors on more localised stress and strain distributions, the stress and strain values were also evaluated within Gruen zones (Gruen et al. 1979).

3. Results

In general, the predicted cement stresses (Figure 2) and bone–cement interface strains (Figure 3) were all higher for the stair ascent load than for the gait load, with elevated values concentrated in the lateral–proximal and medial–distal areas. Figures 4–6 show the effects of the different stem positioning parameters and cement thicknesses considered. (For example, increasing cement thickness reduced von Mises stress and first principal stress at the cement mantle and the equivalent strain in bone at the bone–cement interface). To characterise the overall effect of each factor, the results of all DOE trials for all investigated outputs were collated.

3.1 *Effect of factors*

The variation of each output and the effects of different factors calculated from the main effect analysis (McBurney and White 2010) are summarised in Table 5. A main effect is the effect of an independent variable on a dependent variable averaging across the levels of any other independent variables. The main effect values represent the variance of mean values for three levels of each factor. For example, when ROT_{SI} varies between −5°, 0° and 5°, but all the other factors stay at mean value, the corresponding variance of **Cem-σ_v** is 0.95 MPa for the gait load and 1.43 MPa with stair ascent load.

Table 6 uses pie charts to compare the relative effect of all factors. In terms of relative influence of individual factors (Table 5), ROT_{ML} is the dominant factor for **Cem-σ_v** and **Cem-σ_1** (gait and stairs). For stair ascent, by varying ROT_{ML} from −3° to 3°, the variations of **Cem-σ_v** and **Cem-σ_1** are 1.71, 1.05 MPa relative to 4.97, 2.64 MPa, respectively. The percentages of variations are 34.4% and 39.7%. For **Bone/Cem-ε_v**, ROT_{ML} is the dominant factor with gait load; the effects of ROT_{ML} and TRN_{ML} are almost equal with 36.8% and 38.7% relative to the standard position. In terms of absolute effects of factors in Table 5, all stem position factors have a significant influence on the predicted values. For example, with stair ascent load, the effects of ROT_{SI}, ROT_{ML}, TRN_{AP} and TRN_{ML} on **Bone/Cem-ε_v** are variation ranges of 0.63, 0.76, 0.61 and 0.8 (× 10^3 μ strain), respectively, which are all significant relative to standard value. C_{THICK} has less overall effect on all output measures in all cases.

3.2 *Stress and strain distribution in Gruen zones*

The local variations in different Gruen zones are shown for **Cem-σ_v** (Figure 7) and **Bone/Cem-ε_v** (Figure 8). Peak stress/strain occurs at the distal end of the stem (zone 4).

Table 4. FE output measures for sensitivity study.

Output measure		Location	Units
Cement von Mises stress	**Cem-σ_v**	Throughout cement mantle	MPa
Cement first principal stress	**Cem-σ_1**	Throughout cement mantle	MPa
Bone equivalent strain	**Bone/Cem-ε_v**	At bone–cement interface	10^3 μ strain (10^{-3} strain)

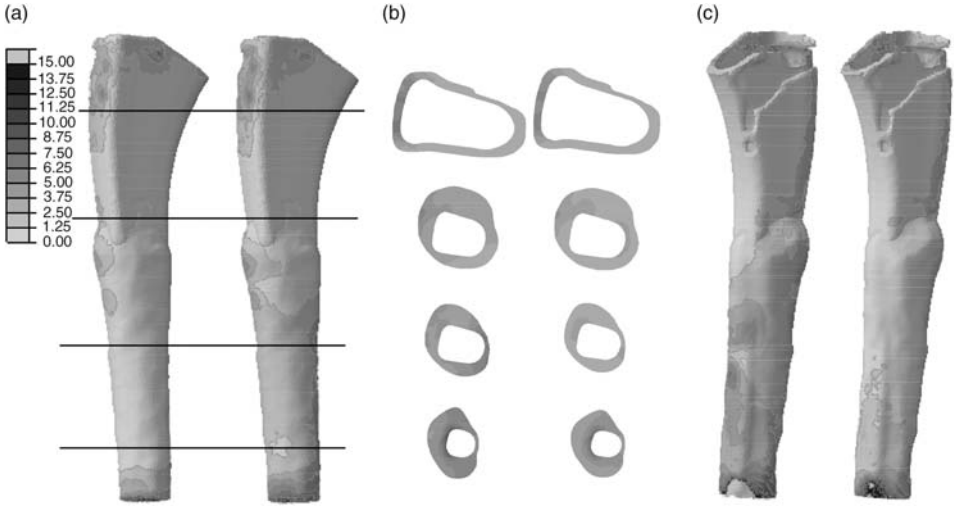

Figure 2. von Mises stress (MPa) in cement mantle during stair ascent (left) and gait (right) of standard stem position (test 25). (a) Front view, right side is medial side; (b) cross-section view in four cutting planes; (c) back view, left side is medial side.

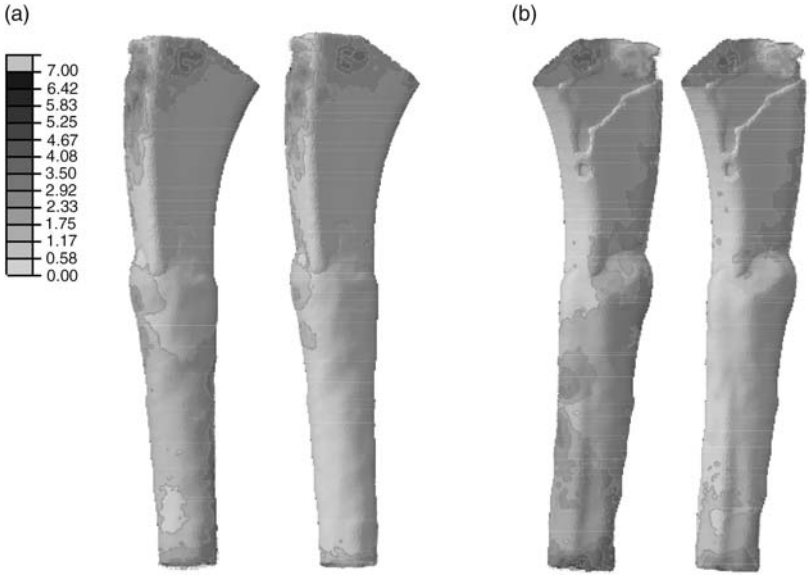

Figure 3. Equivalent strain ($\times 10^3$ μ strain) in bone at bone–cement interface during stair ascent (left) and gait (right) of standard stem position (test 25). (a) Front view, right side is medial side; (b) back view, left side is medial side.

Variations are greatest in the two most proximal zones (1, 7) and the distal zone (4). Again, stresses/strains are higher for stair ascent than gait.

The effects of all factors on stress/strain values are displayed in Tables 7 and 8. For **Cem-σ_v** and **Bone/Cem-ε_v** in all cases, ROT_{ML} is the dominant factor in zones 1, 2, 3, 7; TRN_{AP} and TRN_{ML} are dominant factors in the distal zone 4 and the effect of C_{THICK} is greater in zones 1, 2 and 6 compared to its overall average effect on stress/strain in the whole volume/surface.

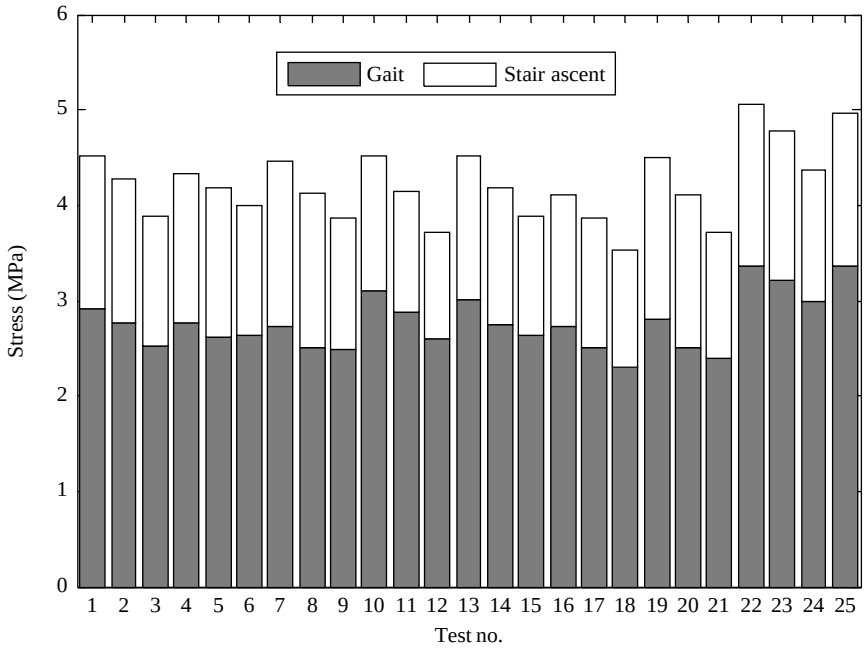

Figure 4. Variation of 95th percentile von Mises stress in cement mantle with gait and stair ascent.

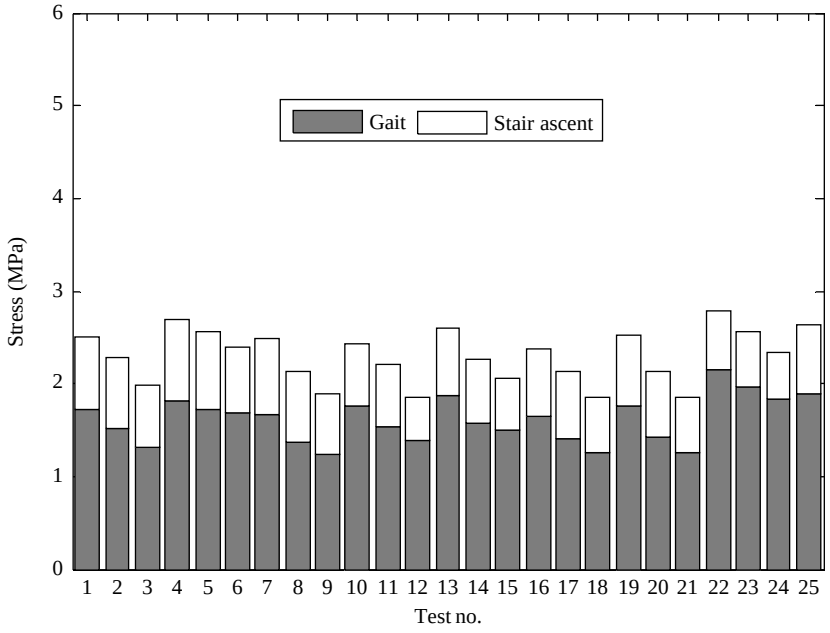

Figure 5. Variation of 95th percentile first principal stress in cement mantle with gait and stair ascent.

4. Discussion

This study investigated the effect of stem position and cement mantle thickness on the stresses and strains within the cement mantle and at the bone–cement interface. For the levels of variation studied, the results clearly show that malpositioning is more influential than cement thickness on the outcomes. In particular, the rotation about the ML axis (which is particularly difficult to detect from 2D coronal radiographs) was highly dominant for all metrics, despite having a lower level of applied variation.

4.1 Corroborating this study against existing work

Before the results are discussed in detail, the important issue of validation of numerical results should be addressed. All numerical models must be properly

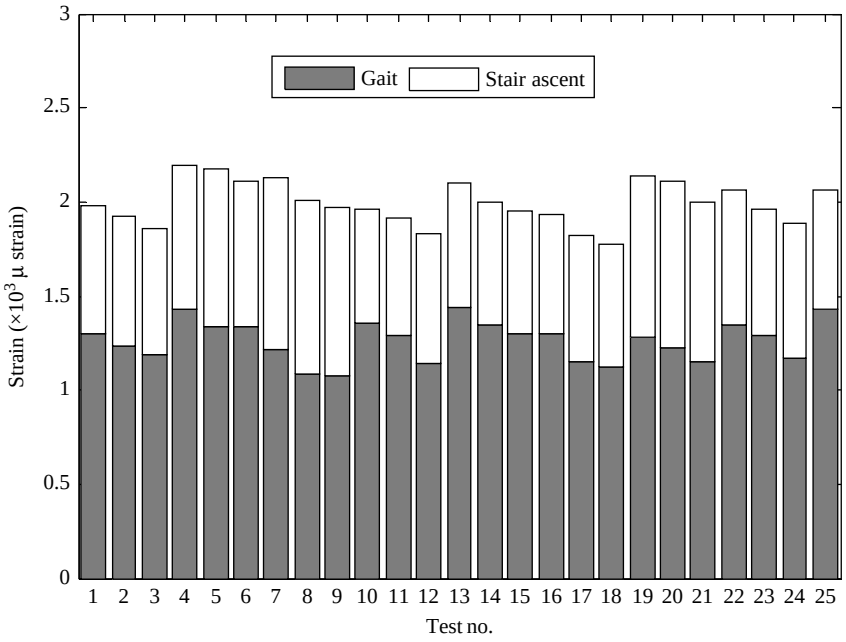

Figure 6. Variation of 95th percentile equivalent strain in bone at bone–cement interface with gait and stair ascent.

Table 5. Main effect of factors (at 95th percentile level) for all investigated outputs.

Output	Load	ROT_{SI}	ROT_{ML}	TRN_{AP}	TRN_{ML}	C_{THICK}
Cem-σ_v (Mpa)	Gait (3.36)	0.95 (28.27%)	1.19 (35.42%)	1.04 (30.95%)	0.66 (19.64%)	0.32 (9.52%)
	Stair (4.97)	1.43 (28.77%)	1.71 (34.41%)	1.6 (32.19%)	1.18 (23.74%)	0.56 (11.27%)
Cem-σ_1 (MPa)	Gait (1.89)	0.55 (29.14%)	0.83 (43.97%)	0.6 (31.79%)	0.37 (19.60%)	0.33 (17.48%)
	Stair (2.64)	0.68 (25.78%)	1.05 (39.81%)	0.83 (31.47%)	0.72 (27.30%)	0.47 (17.82%)
Bone/Cem-ε_v (10^3 μ strain)	Gait (1.43)	0.38 (26.55%)	0.56 (39.13%)	0.41 (28.65%)	0.42 (29.35%)	0.13 (9.08%)
	Stair (2.07)	0.63 (30.49%)	0.76 (36.78%)	0.61 (29.52%)	0.8 (38.72%)	0.12 (5.81%)

Notes: In load column, the values in brackets are output when stem in neutral position (test 25); in the factor columns, main effects of factors are listed, the values in brackets are relative percentile of these main effects relative to standard value in load column.

validated in order to provide useful information. In the present case, the purpose of this sensitivity study is to lay the groundwork for this FE model to be validated in more detail against patient-specific clinical follow-up data (this will be the subject of a subsequent publication). Nonetheless, it is still helpful at this juncture to consider how the modelling work compares to the validated FE studies of the implanted hip.

In tis study, the output measures monitored are stress levels within the cement and surface strain at the bone–cement interface. Volumetric measures cannot easily be reproduced experimentally, but studies have attempted to characterise surface strains in particular.

Ramos et al. (2012) used optical fibre Bragg grating sensors to measure strains *within* the cement mantle, and found that strains could vary considerably across the cement, from the proximal to distal regions. Whilst high concentrations of strain were reported around the distal region (as in this study), high values could also occur in the mid-region or proximally. A similar trend was found by Rohlmann et al. (1983), who reported considerable variations in the strains depending on location, but generally larger values at the distal zone. Stolk et al. (2002) also found generally higher strains at the most distal measurement locations.

Fewer studies have experimentally varied factors under test, but those that have are in agreement with this study. Fisher et al. (1997) used embedded strain gauges to monitor the cement mantle for different thicknesses of cement, and found reduced strains for a thicker mantle, as is consistently apparent in the present numerical study.

FE models of cemented THR have previously been widely used to determine the stress distribution in the bulk cement or at the cement interface (Mann et al. 1995; Lennon and Prendergast 2001; Stolk et al. 2001). Some studies have compared the performance of different designs (Mann et al. 1997; Janssen et al. 2005; Abdullah et al. 2010), other studies have compared the stress

Table 6. Pie-chart plot of main effect for all outputs.

Output	Gait		Stair ascent
Cem-σ_v	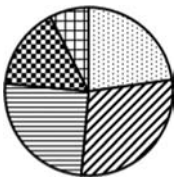		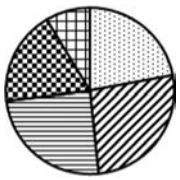
Cem-σ_1		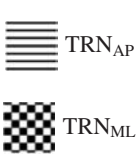	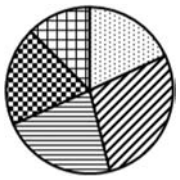
Bone/Cem-ε_v			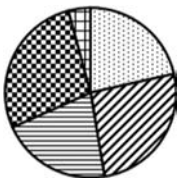

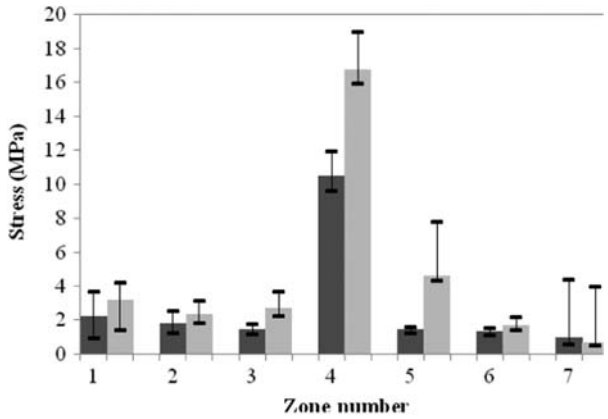

Figure 7. Variation of 95th percentile von Mises stress in cement mantle. Dark bars represent gait, light bars represent stair ascent; the filled bar represents outputs of standard stem position (test 25), the error bar plot represents variation of output values.

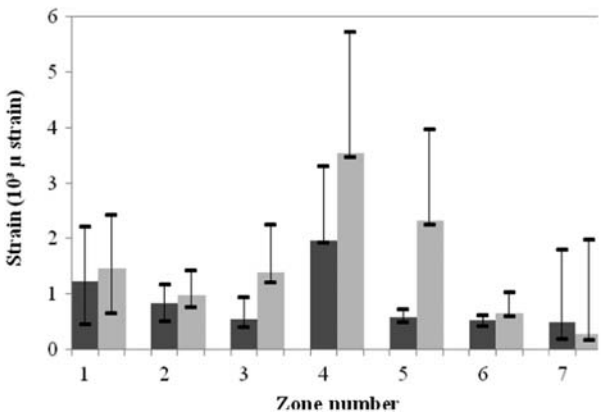

Figure 8. Variation of 95th percentile equivalent strain in bone at bone–cement interface. Dark bars represent gait, light bars represent stair ascent; the filled bar represents outputs of standard stem position (test 25), the error bar plot represents variation of output values.

distribution with bonded and debonded cement–stem interfaces (Chang et al. 1998; Lennon and Prendergast 2001; Pérez et al. 2006). Pérez et al. (2006) analysed the influence of the bonding degree of the stem–cement interface on the failure probability of cemented hip prostheses. It was predicted that critical sites appeared at the different regions with different stem–cement interface conditions. The critical regions were found at the distal and proximal regions of the cement mantle with a debonded stem–cement interface. Lennon and Prendergast (2001) evaluated cement stresses in cemented THR with different stem–cement interface conditions, and concluded that the stressed volume should be used as measure of durability of cement fixation. They predicted high stresses in the proximal medial region and the region surrounding the distal tip. However, the FE model was a composite femur and loads were only applied on the greater trochanter. Jonkers et al. (2008) developed a patient-specific FE model of the proximal femur and applied muscle loads using a musculoskeletal model. The von Mises stresses on the

Table 7. Pie-chart plot of main effect for **Cem-σ_v** in Gruen zones.

Zone number	Gait		Stair ascent
1	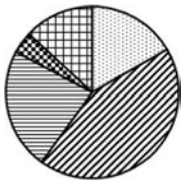		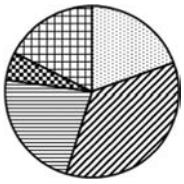
2	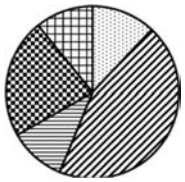		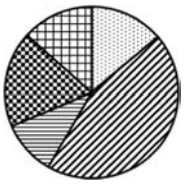
3	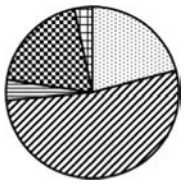		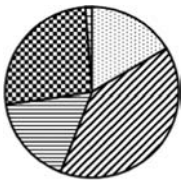
4	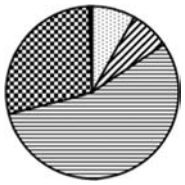		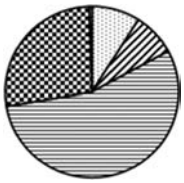
5	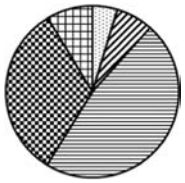		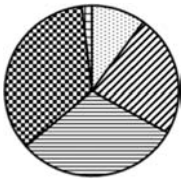
6	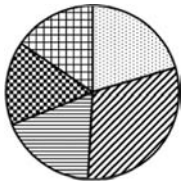		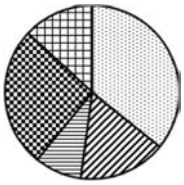
7	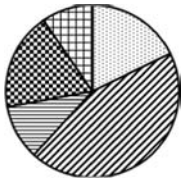		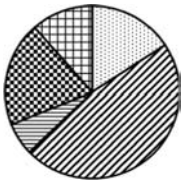

Table 8. Pie-chart plot of main effect for **Bone/Cem-ε_v** in Gruen zones.

Zone number	Gait	Stair ascent
1	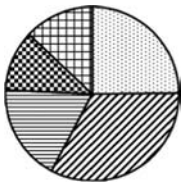	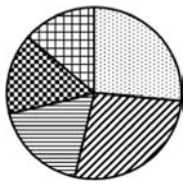
2	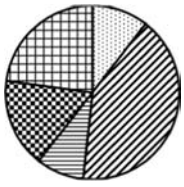	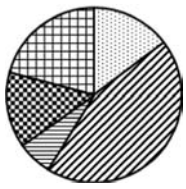
3	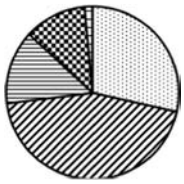	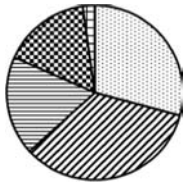
4	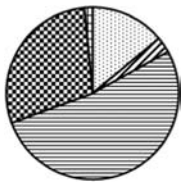	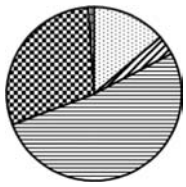
5	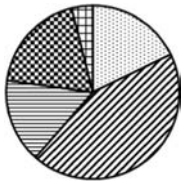	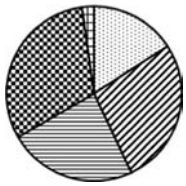
6	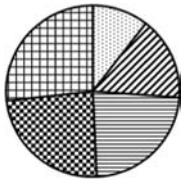	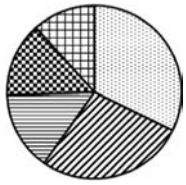
7	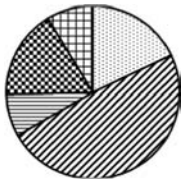	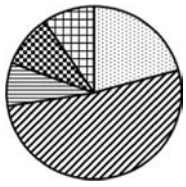

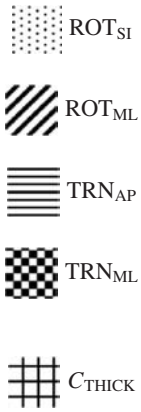

lateral proximal femur were equal to or higher than those on the medial proximal femur. Another reason for the higher stress and strain in the lateral proximal femur is the relatively low density in this area for this patient. Nicolella et al. (2006) performed a probabilistic analysis to assess the effect of three-dimensional (3D) deterministic shape optimisation of a cemented femoral prosthesis on the predicted probability of failure of the prosthesis system. It was found that the uncertainty in the joint loading, cement strength and implant–cement interface strength have the greatest effect on the computed probability of failure. Stolk et al. (2001) used FE to investigate the sensitivity of THR stress and strain fields to joint and muscle forces, and reported that the hip-joint contact forces and abductor forces were the most influential factors.

Comparisons of previous works with this study must account for the different factors and different implants being investigated. Ramaniraka et al. (2000) evaluated micromotion and stress at the cement–bone and cement–stem interfaces for titanium and cobalt-chromium stems. They found that micromotion was minimal with a cement mantle 3–4 mm thick but then increased with greater cement thickness. They also found abnormally high micromotions when the cement was thinner than 2 mm and the stem was made of titanium. For a cobalt-chromium stem, the variations of stresses at both interfaces did not vary significantly as a function of cement mantle thickness. This latter result is consistent with the findings of this study. Ramaniraka et al. (2000) assumed that both the cement–bone and cement–stem interfaces were debonded. However, the cement–bone interface was bonded in the current study, as cement and cancellous bone were assumed to be integrated as a composite. Kleemann et al. (2003) simulated the effect of femoral anteversion and offset in cemented THR, and found that femoral anteversion was more critical. Although it is hard to perform direct comparisons, as a different anteversion range was used and other stem position factors were not included in Kleemann's study, they also concluded that ROT_{SI} is the main factor influencing cement mantle stresses. Looking at the different Gruen zones (Table 7), both Kleemann's study and this study predicted higher sensitivity of cement stress to ROT_{SI} in the medial–proximal zone (Gruen zone 7) as compared to the medial–distal zones (Gruen zones 4 and 5).

The sensitivity to cement thickness was lower than the sensitivity to stem positioning. A number of experimental studies appear to demonstrate that the total femoral cement mantle including pure cement and the cement interdigitated into the cancellous bone must be at least 3 mm thick to reduce risks of cement fatigue; thin and deficient mantles have been associated with adverse results (Hernigou et al. 2009). Ramaniraka et al. (2000) suggested an optimum thickness of cement was in the range of 3-5 mm. Huiskes (1990) recommended a non-uniform thickness of cement ranging from 3 to 6 mm for the proximal part of the canal. However, from Hernigou's (2009) review, the thickness of the cement mantle does not appear to have an influence on the risk of loosening beyond 10 years post-operatively (Ramaniraka et al. 2000), suggesting that late loosening is related to an absence of primary stability of the implant rather than cement mantle thickness. The range of cement thickness was 2–4 mm in this study, and is comparable to the suggested 'good' ranges in the literature. This may be the reason that stress/strain sensitivity is lower for cement thickness than for other factors. The sensitivity of cement thickness may increase outside the range investigated. Another possibility for the low sensitivity is that the cement thickness is effectively constant in the distal region due to the filling of the medullary cavity. This can be observed from Tables 7 and 8 (the very low effect of C_{THICK} in the distal zones 3–5).

Considering the local stress/strain distributions in the Gruen zones, high stresses in the cement mantle and high strains in bone at the bone–cement interface were found in the proximal (Gruen zone 1) and distal (Gruen zones 3–5) areas of the stem. This is consistent with other studies (Stolk et al. 2001; Jonkers et al. 2008).

Looking at different Gruen zones, the effects of factors in individual zones do differ from the overall effect across the whole cement mantle. ROT_{ML} is dominant in the proximal zone, TRN_{AP} and TRN_{ML} are dominant factors at the distal end of cement mantle.

Only the peak forces associated with gait and stair ascent were investigated in this study, since these are considered most relevant. Pérez et al. (2006) analysed the influence of the stem–cement bonding degree on the performance of cemented hip prostheses. From the two cases analysed, stair ascent was predicted to be more detrimental than gait loading. The same conclusion was drawn by Kleemann et al. (2003). This is in agreement with this study also.

'Peak' values were represented using the 95th percentile instead of the maximum value in the FE model, since individual maxima in elements are prone to numerical artifacts and singularities. In theory, FE is able to determine the stresses in the cement and hence the durability of the implant fixation. However, a significant problem is that the stress distribution in a cement mantle around an orthopaedic implant is complex. The true bone microstructure and also the cement composition (e.g. influence of cement porosity) will affect the localised stress concentrations (Harrigan et al. 1992). In this respect, monitoring the peak stress (as in this study) may give an incorrect picture of the potential durability of the cemented fixation.

This study has a number of limitations. Only two load cases (gait and stair ascent) were considered in this study, as compared to the spectrum of loading likely to be

experienced during activities of daily living. Both cancellous and cortical bone were modelled as elastic and isotropic, as opposed to anisotropic (Ciarelli et al. 1991; Keaveny et al. 2001), and the failure-criterion is not well-defined for these materials. Cement was also modelled as elastic and isotropic, the viscoelastic properties and initial damage (voids, cracks originated by initial residual stresses) were neglected (Lewis 1998; Jeffers et al. 2007). Bone–cement composite properties were calculated based on bone porosity; true mechanical properties of the composite are more complex (Waanders et al. 2010). The bone properties are based on pre-operative CT data; in reality, bone dynamically adapts and remodels over time, so the results will not reflect the longer-term performance of the THR. The levels of variation studied for the input factors are estimates only, based on alignment tolerances judged by visual inspection. It is clear from the results that the magnitude of these values is important, so understanding these uncertainties is essential if patient-specific FE models are to move closer to being accurate, verifiable tools for clinical case-study use.

5. Conclusions

The sensitivity of THR to uncertainty in stem positioning and cement thickness was investigated using FE analysis, based on the recognised difficulties of estimating these parameters from limited medical imaging data. Mal-rotations and mal-translations were found to dominate the sensitivity analysis, with cement thickness emerging as less influential. The effect of these factors was found to be reasonably consistent for both gait and stair ascent load-cases. The variations were most pronounced in the most proximal and distal zones around the stem (i.e. at the extremities). The levels of observed variation are large enough to mask other effects which may be studied in a patient-specific FE model. Therefore, it is very important for researchers working on patient-specific models using clinical data to ensure that particular attention is given to ensuring that the out-of-plane positioning has been accurately assessed, and where this uncertainty cannot be easily resolved, performing comparable sensitivity studies to this one to ensure that the influence of that uncertainty can be quantified and accounted for in subsequent analyses. Clinically, this study once again reaffirms the absolutely central importance of effective alignment, and demonstrates that assessment of 2D radiographic images alone does not provide a full and comprehensive assessment of the 3D alignment and its influence on implant performance.

Acknowledgements

The research leading to these results has received funding from the European Information and Communication Technologies Community Seventh Framework Programme (FP7) under Grant agreement no. 248693.

Notes

1. Email: j.shi@soton.ac.uk
2. Email: ams05@alumni.soton.ac.uk
3. Email: gunnar.flivik@med.lu.se
4. Email: mark.taylor@flinders.edu.au

References

Abdullah AH, Asri MNM, Alias MS, Giha T. 2010. Finite element analysis of cemented hip arthroplasty: influence of stem tapers. Lect Notes Eng Comp Sci. 2241–2246.

Bah MT, Nair PB, Taylor M, Browne M. 2011. Efficient computational method for assessing the effects of implant positioning in cementless total hip replacements. J Biomech. 44(7):1417–1422.

Bergmann G, Graichen F, Rohlmann A. 1993. Hip joint loading during walking and running, measured in two patients. J Biomech. 26(8):969–990.

Chang PB, Mann KA, Bartel DL. 1998. Cemented femoral stem performance. Effects of proximal bonding, geometry, and neck length. Clin Orthop Relat Res. 355:57–69.

Ciarelli MJ, Goldstein SA, Kuhn JL, Cody DD, Brown MB. 1991. Evaluation of orthogonal mechanical-properties and density of human trabecular bone from the major metaphyseal regions with materials testing and computed-tomography. J Orthop Res. 9(5):674–682.

Coultrup O. 2010. The computational assessment of mechanical fixation failure in cemented total hip arthroplasty. University of Southampton.

Dopico-Gonzalez C, New AM, Browne M. 2010. Probabilistic finite element analysis of the uncemented hip replacement-effect of femur characteristics and implant design geometry. J Biomech. 43(3):512–520.

Fisher DA, Tsang AC, Paydar N, Milionis S, Turner CH. 1997. Cement-mantle thickness affects cement strains in total hip replacement. J Biomech. 30(11–12):1173–1177.

Gruen TA, Mcneice GM, Amstutz HC. 1979. Modes of failure of cemented stem-type femoral components – radiographic analysis of loosening. Clin Orthop Relat Res. 141:17–27.

Harrigan TP, Kareh JA, Oconnor DO, Burke DW, Harris WH. 1992. A finite-element study of the initiation of failure of fixation in cemented femoral total hip components. J Orthop Res. 10(1):134–144.

Harrington MA, O'Connor DO, Lozynsky AJ, Kovach I, Harris WH. 2002. Effects of femoral neck length, stem size, and body weight on strains in the proximal cement mantle. J Bone Joint Surg Am. 84A(4):573–579.

Heller MO, Bergmann G, Kassi JP, Claes L, Haas NP, Duda GN. 2005. Determination of muscle loading at the hip joint for use in pre-clinical testing. J Biomech. 38(5):1155–1163.

Herberts P, Malchau H. 1997. How outcome studies have changed total hip arthroplasty practices in Sweden. Clin Orthop Relat Res. 344:44–60.

Herberts P, Malchau H. 2000. Long-term registration has improved the quality of hip replacement – a review of the Swedish THR Register comparing 160,000 cases. Acta Orthop Scand. 71(2):111–121.

Hernandez CJ, Beaupre GS, Keller TS, Carter DR. 2001. The influence of bone volume fraction and ash fraction on bone strength and modulus. Bone. 29(1):74–78.

Hernigou P, Daltro G, Lachaniette CH, Roussignol X, Mukasa MM, Poignard A. 2009. Fixation of the cemented stem: clinical relevance of the porosity and thickness of the cement mantle. Open Orthop J. 3:8–13.

Huiskes R. 1990. The various stress patterns of press-fit, ingrown, and cemented femoral stems. Clin Orthop Relat Res. 261:27–38.

Isaac GH, Busch CA, Shetty V, Drabu KJ. 2000. Radiographic assessment of the cement mantle thickness of the femoral stem in total hip replacement: a case study of 112 consecutive implants. Proc Inst Mech Eng H. 214(5):471–477.

Ishida T, Nishimura I, Tanino H, Higa M, Ito H, Mitamura Y. 2011. Use of a genetic algorithm for multiobjective design optimization of the femoral stem of a cemented total hip arthroplasty. Artif Organs. 35(4):404–410.

Janssen D, Aquarius R, Stolk J, Verdonschot N. 2005. The contradictory effects of pores on fatigue cracking of bone cement. J Biomed Mater Res B Appl Biomater. 74(2):747–753.

Jeffers JRT, Browne M, Lennon AB, Prendergast PJ, Taylor M. 2007. Cement mantle fatigue failure in total hip replacement: experimental and computational testing. J Biomech. 40(7):1525–1533.

Jonkers I, Sauwen N, Lenaerts G, Mulier M, Van der Perre G, Jaecques S. 2008. Relation between subject-specific hip joint loading, stress distribution in the proximal femur and bone mineral density changes after total hip replacement. J Biomech. 41(16):3405–3413.

Keaveny TM, Morgan EF, Niebur GL, Yeh OC. 2001. Biomechanics of trabecular bone. Annu Rev Biomed Eng. 3:307–333.

Kleemann RU, Heller MO, Stoeckle U, Taylor WR, Duda GN. 2003. THA loading arising from increased femoral anteversion and offset may lead to critical cement stresses. J Orthop Res. 21(5):767–774.

Kovanda M, Havlicek V, Hudec J. 2009. Mathematical simulation of stem/cement/bone mechanical interactions for Poldi-Cech, CF-30, MS-30 and PFC femoral components. Acta Chir Orthop Traumatol Cech. 76(2):110–115.

Kumar YSA, Pant B, Singh KD. 2009. Thickness effects on maximum von-Mises stress of a cement mantle in total hip replacement – a finite element study. J Appl Biomater Biomech. 7(2):111–115.

Lengsfeld M, Burchard R, Gunther D, Pressel T, Schmitt J, Leppek R, Griss P. 2005. Femoral strain changes after total hip arthroplasty – patient-specific finite element analyses 12 years after operation. Med Eng Phys. 27(8):649–654.

Lennon AB, Britton JR, MacNiocaill RF, Byrne DP, Kenny PJ, Prendergast PJ. 2007. Predicting revision risk for aseptic loosening of femoral components in total hip arthroplasty in individual patients – a finite element study. J Orthop Res. 25(6):779–788.

Lennon AB, Prendergast PJ. 2001. Evaluation of cement stresses in finite element analyses of cemented orthopaedic implants. J Biomech Eng-T ASME. 123(6):623–628.

Lewis G. 1997. Properties of acrylic bone cement: state of the art review. J Biomed Mater Res. 38(2):155–182.

Lucksanasombool P, Higgs WAJ, Ignat M, Higgs RJED, Swain MV. 2003. Comparison of failure characteristics of a range of cancellous bone–bone cement composites. J Biomed Mater Res A. 64A(1):93–104.

Mann KA, Bartel DL, Ayers DC. 1997. Influence of stem geometry on mechanics of cemented femoral hip components with a proximal bond. J Orthop Res. 15(5):700–706.

Mann KA, Bartel DL, Wright TM, Burstein AH. 1995. Coulomb frictional interfaces in modeling cemented total hip replacements – a more realistic model. J Biomech. 28(9):1067–1078.

Massoud SN, Hunter JB, Holdsworth BJ, Wallace WA, Juliusson R. 1997. Early femoral loosening in one design of cemented hip replacement. J Bone Joint Surg Br. 79B(4):603–608.

Morgan EF, Bayraktar HH, Keaveny TM. 2003. Trabecular bone modulus–density relationships depend on anatomic site. J Biomech. 36(7):897–904.

Morgan EF, Keaveny TM. 2001. Dependence of yield strain of human trabecular bone on anatomic site. J Biomech. 34(5):569–577.

Nalla RK, Kinney JH, Ritchie RO. 2003. Mechanistic fracture criteria for the failure of human cortical bone. Nat Mater. 2(3):164–168.

Nicolella DP, Thacker BH, Katoozian H, Davy DT. 2006. The effect of three-dimensional shape optimization on the probabilistic response of a cemented femoral hip prosthesis. J Biomech. 39(7):1265–1278.

Pancanti A, Bernakiewicz M, Viceconti M. 2003. The primary stability of a cementless stem varies between subjects as much as between activities. J Biomech. 36(6):777–785.

Pérez MA, Garcia-Aznar JM, Doblare M. 2009. Does increased bone–cement interface strength have negative consequences for bulk cement integrity? A finite element study. Ann Biomed Eng. 37(3):454–466.

Pérez MA, Grasa J, Garcia-Aznar JM, Bea JA, Doblare M. 2006. Probabilistic analysis of the influence of the bonding degree of the stem–cement interface in the performance of cemented hip prostheses. J Biomech. 39(10):1859–1872.

Perillo-Marcone A, Ryd L, Johnsson K, Taylor M. 2004. A combined RSA and FE study of the implanted proximal tibia: correlation of the post-operative mechanical environment with implant migration. J Biomech. 37(8):1205–1213.

Ramaniraka NA, Rakotomanana LR, Leyvraz PF. 2000. The fixation of the cemented femoral component. Effects of stem stiffness, cement thickness and roughness of the cement–bone surface. J Bone Joint Surg Br. 82(2):297–303.

Ramos A, Schiller MW, Abe I, Lopes PA, Simões JA. 2012. Experimental measurement and numerical validation of bone cement mantle strains of an *in vitro* hip replacement using optical FBG sensors. ~~Exp Mech. 1–8.~~ [Q11]

Rohlmann A, Mössner U, Bergmann G, Kölbel R. 1983. Finite-element-analysis and experimental investigation in a femur with hip endoprosthesis. J Biomech. 16(9):727–742.

Schileo E, Taddei F, Malandrino A, Cristofolini L, Viceconti M. 2007. Subject-specific finite element models can accurately predict strain levels in long bones. J Biomech. 40(13):2982–2989.

Star MJ, Colwell CW, Jr, Kelman GJ, Ballock RT, Walker RH. 1994. Suboptimal (thin) distal cement mantle thickness as a contributory factor in total hip arthroplasty femoral component failure. A retrospective radiographic analysis favoring distal stem centralization. J Arthroplasty. 9(2):143–149.

Stolk J, Maher SA, Verdonschot N, Prendergast PJ, Huiskes R. 2003. Can finite element models detect clinically inferior cemented hip implants? Clin Orthop Relat Res. 409:138–150.

Stolk J, Verdonschot N, Cristofolini L, Toni A, Huiskes R. 2002. Finite element and experimental models of cemented hip joint reconstructions can produce similar bone and cement strains in pre-clinical tests. J Biomech. 35(4):499–510.

Stolk J, Verdonschot N, Huiskes R. 2001. Hip-joint and abductor-muscle forces adequately represent *in vivo* loading of a cemented total hip reconstruction. J Biomech. 34(7):917–926.

Stone JJS, Rand JA, Chiu EK, Grabowski JJ, An KN. 1996. Cement viscosity affects the bone–cement interface in total hip arthroplasty. J Orthop Res. 14(5):834–837.

Taylor D. 2003. Fracture mechanics – how does bone break? Nat Mater. 2(3):133–134.

Taylor M, Tanner KE, Freeman MAR. 1998. Finite element analysis of the implanted proximal tibia: a relationship between the initial cancellous bone stresses and implant migration. J Biomech. 31(4):303–310.

The B, Hosman A, Kootstra J, Kralj-Iglic V, Flivik G, Verdonschot N, Diercks R. 2008. Association between contact hip stress and RSA-measured wear rates in total hip arthroplasties of 31 patients. J Biomech. 41(1):100–105.

Turner AWL, Gillies RM, Sekel R, Morris P, Bruce W, Walsh WR. 2005. Computational bone remodelling simulations and comparisons with DEXA results. J Orthop Res. 23(4):705–712.

Van Goethem C, Pfluger DH. 2005. Assessment of early migration and clinical evaluation of a cemented femoral stem. Acta Orthop Belg. 71(5):555–564.

Verdonschot N, Huiskes R. 1997. The effects of cement–stem debonding in THA on the long-term failure probability of cement. J Biomech. 30(8):795–802.

Viceconti M, Muccini R, Bernakiewicz M, Baleani M, Cristofolini L. 2000. Large-sliding contact elements accurately predict levels of bone–implant micromotion relevant to osseointegration. J Biomech. 33(12):1611–1618.

Waanders D, Janssen D, Mann KA, Verdonschot N. 2010. The mechanical effects of different levels of cement penetration at the cement–bone interface. J Biomech. 43(6):1167–1175.

Waanders D, Janssen D, Mann KA, Verdonschot N. 2011. The behavior of the micro-mechanical cement–bone interface affects the cement failure in total hip replacement. J Biomech. 44(2):228–234.